ACS OMEGA

Open Access

http://pubs.acs.org/journal/acsodf

Article

Cellulose Nanomaterials Functionalized with Carboxylic Group Extracted from Lignocellulosic Agricultural Waste: Isolation and Cu(II) Adsorption for Antimicrobial Application

Thai Anh Do, Anh Tuyet Phung Thi, Thi Huong Le, Dang Do Van, Thoa Nguyen Kim, and Quyen Van Nguyen*

Cite This: *ACS Omega* 2025, 10, 6234−6243

Read Online

ACCESS | Metrics & More | Article Recommendations | Supporting Information

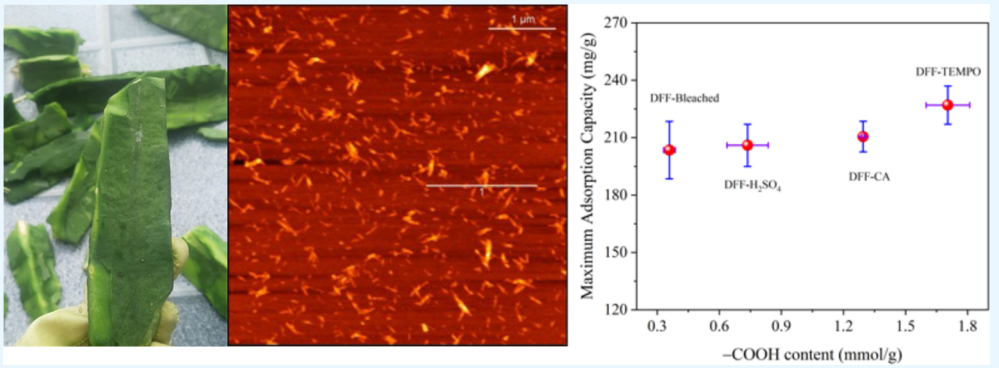

ABSTRACT: In this study, we reported the isolation of COOH-functionalized nanocrystal cellulose from agricultural waste, particularly dragon fruit foliage (DFF), by two methods, the citric acid/HCl acid (CA) method and the (2,2,6,6-tetramethylpiperidin-1-yl)oxyl (TEMPO)-mediated oxidation method. Chemical component quantification and physiochemical characterization techniques, such as FT-IR spectroscopy, XRD, TGA, XPS, and AFM, were employed to analyze DFF, bleached cellulose, and extracted CNs. We determined the contents of lignin and hemicellulose removed, while the signals for the cellulose contents remain the same for DFF-CA and DFF-TEMPO. The DLS, AFM, and SEM results indicated that the DFF-CA sample has a smaller average particle size (250 ± 50 nm) with a rod-like shape, compared to the DFF-TEMPO sample (600 ± 100 nm) with a fiber-like shape. Importantly, CNs extracted from DFF, including DFF-TEMPO, DFF-CA, and DFF-bleached, exhibited excellent properties for Cu (II) adsorption with a maximum adsorption of 227 $mg{\cdot}g^{-1}$ (for DFF-CA samples), and the adsorption is almost independent of the −COOH content. Notably, we were also able to prepare Cu-containing cellulose gels showing promising antimicrobial activity. Our work opens new possibilities for the use of unexplored cellulosic byproducts in the agricultural industry as well as potential applications of Cu-containing cellulose gels as antimicrobials.

INTRODUCTION

Cellulose-based nanomaterials (CNs) have been considered as one of the most promising bioderived nanomaterials since they have a variety of unique properties; for example, they can be naturally degraded, regenerated in the biosphere, and are especially environmentally friendly.[1−9] Cellulose nanomaterials or nanocrystal cellulose (CN), with the $(C_6H_5O_6)_n$ chemical formula, are forms of cellulose in which at least one of its dimensions is at the nanoscale. For example, CNs can be shaped as nanorods with an aspect ratio (length/width) less than 50, while nanofibers have an aspect ratio greater than 100.[10,11] CNs are produced by hydrolyzing cellulosic wood by various chemical methods; for example, mineral acid at a pilot scale[12−14] and organic acids[15−17] or ionic liquids at a lab scale.[18−20] The chemical method is of interest because it not only allows a high yield of the reaction but also provides the possibility to control the surface chemistry of CNs, which in turn affects the dispersion of CNs in water and enable CNs in several applications.[21−24] For example, hydrolyzing cellulose by H_2SO_4 will generate CN functionalized with the $-O-SO_3^-$ sulfate group, while the reaction of cellulose with organic acids will produce CN functionalized with the carboxylic acid, −COOH, functional group.[7,25]

Received: December 20, 2024
Revised: January 22, 2025
Accepted: January 27, 2025
Published: February 5, 2025

As important as the method of producing CNs is the cellulosic or lignocellulose source, which could be woody or nonwoody sources. However, there is still a variety of cheap, unexplored cellulosic waste materials in especially agricultural residues, fruit waste, and vegetable waste. Among them, dragon fruit or pitaya, shown in Figure 1, is native to tropical regions

Figure 1. Procedures to extract nanocellulose from dragon fruit foliage by different approaches including (2,2,6,6-tetramethylpiperidin-1-yl)oxyl (TEMPO) and citric acid.

and has been widely grown in provinces and cities throughout the country over more than 55,000 ha in Vietnam. Dragon fruit foliage (DFF), which was estimated at approximately 10^6 tons per year, is considered one of the agricultural byproducts obtained by pruning dragon fruit trees and is mostly treated as agricultural waste in Vietnam. Importantly, DFF is fast-growing, inexpensive, renewable, sustainable, and has a high rate of reproduction; this makes DFF an interesting byproduct source to extract CNs.

Cellulose nanomaterials have been widely explored in many research areas, such as wastewater bioadsorbent,[26,27] energy storage,[28] oil recovery,[29] biomedical field,[30] antimicrobial agent,[31,32] and food additives.[33] Interestingly, the properties of CNs are usually strongly dependent on the surface chemistry of the CNs. Recently, Liu et al. reported that the maximum adsorption capacity of Cu(II) on carboxylic acid-functionalized CNs was 75 $mg{\cdot}g^{-1}$, and the adsorption of Cu(II) onto modified CNs was extremely fast, reaching equilibrium within a few minutes, and the adsorption capacity strongly depended on the content of the −COOH group.[34] Qin et al. later reported a record high equilibrium Cu^{2+} removal capacity of 115.3 $mg{\cdot}g^{-1}$ and attributed it to the high −COOH content.[35] Valencia et al. also reported the use of CNs functionalized with the −COOH group as a support substance to spontaneously form metal oxide nanoparticles, Cu_2O, on its −COOH surface.[36] They also observed that these hybrid nanomaterials between Cu_2O and nanocrystal cellulose can be used as antimicrobial materials, which is important since it opens a new and simple approach to convert "inactive" cellulose materials into "active" materials.[36] Generally, copper exhibits antimicrobial properties through various mechanisms, including the generation of reactive oxygen species (ROS), disruption of cell membranes, and binding to essential cellular components such as DNA and proteins, leading to cell death and inhibition of microbial growth.[37] As a result, copper-containing materials can be utilized in various applications, such as in medical settings, to reduce infection rates or agricultural uses for fungicidal protection of crops.[37−40] Cu(II)-containing cellulose has usually been prepared based on the hypothesis that there is a strong affinity of Cu(II) and the −COOH group on the surface.[41−43] However Magallanes et al. recently used X-ray photoemission spectroscopy (XPS) to detect Cu^{2+} cations adsorbed on a self-assembled monolayer of carboxylic acid and alcohol-terminated thiol molecules, and they reported that the affinity of Cu^{2+} toward the −COOH and −OH groups was similar,[44] which was in contradiction to the Cu^{2+} adsorption results.

Here, we selected DFF as the lignocellulosic source to produce a COOH-functionalized nanocrystal cellulose, as illustrated in Figure 1. The chemical components of DFF, bleached cellulose, and CNs will be quantified, and the physicochemical properties of all samples will be characterized using various techniques. We also studied the adsorption of Cu(II) on COOH-functionalized cellulose nanomaterials to investigate the affinity of −OH and −COOH groups toward Cu(II). We observed that the Cu(II) adsorption is fast, strong, and weakly dependent on the −COOH content and, more importantly, this Cu-containing cellulose gel shows promising antimicrobial activities.

EXPERIMENTAL SECTION

Chemicals. Finely dried DFF was obtained by mechanically milling air-dried DFF, which was then stored in a sealed container. Analytical-grade chemicals including sodium hydroxide, hydrogen peroxide, acetic acid, (2,2,6,6-tetramethylpiperidin-1-yl)oxyl (TEMPO), sodium bromide, sodium hypochlorite solution, citric acid (CA), $Cu(NO_3)_2$ salt, and hydrochloric acid were purchased from Sigma-Aldrich and used without further purification.

Isolation of Carboxylate Cellulose Nanomaterials (CCNs). CCNs were produced from bleached cellulose using two methods, as illustrated in Figure 1. First, bleached DFF was obtained after several steps including chemical treatments with 3% NaOH followed by a solution of H_2O_2 (1.3%, w/w) and acetic acid (0.1%, v/v); more details can be found in our previous report[45] and in the bleaching step in Figure 1.

The first method was based on acid hydrolysis catalyzed by a mixture of citric acid and HCl. The bleached cellulose was dispersed in the acid mixture (90% citric acid (3 M, v/v)/10% HCl (6 M, v/v)) in a ratio of 1:50 at 80 °C for 4 h with continuous stirring (400 rpm). To enhance the dispersion of the bleached DFF, the initial suspension was sonicated using an Elmasonic S 300H instrument for 20 min. To terminate the reaction, the suspension was rapidly cooled to room temperature by adding distilled water to quench the hydrolysis reaction. The CNs labeled DFF-CA were then washed with deionized water several times by centrifugation at 9000 rpm for 10 min until they reached a neutral pH.

The second method was to use (2,2,6,6-tetramethylpiperidin-1-yl) oxyl as an oxidative agent, as well-documented previously.[46,47] First, 2 g of the bleached DFF cellulose was suspended in 200 mL of deionized water, including 0.025 g of

https://doi.org/10.1021/acsomega.4c11464
ACS Omega 2025, 10, 6234−6243

TEMPO and 0.25 g of NaBr, and then sonicated for 20 min with an Elmasonic S 300H instrument to improve dispersion. The oxidation process was started by adding NaClO 8% (2.42 mmol/g) at a rate of 400 rpm and at room temperature. The pH was stabilized at 10−10.5 by adding NaOH at 0.5 M until no change in pH was observed. Afterward, the suspension was neutralized by adding 0.5 M HCl. TEMPO-oxidized fiber (DFF-TEMPO) was centrifuged at 9000 rpm for 10 min to collect the precipitate and then redispersed in deionized water using a high-intensity ultrasonic processor (UP200 St, Hielscher). The suspension obtained was kept at 4 °C for the next experiment.

Materials Characterization. The chemical structure of the samples was determined by Fourier transform infrared (FT-IR) spectroscopy (FT/IR 4700, JASCO, Japan) in attenuated total reflectance mode in the wavenumber range of 400−4000 cm^{-1} with a step of 2 cm^{-1} and for 32 scans. The thermal stability of the samples was evaluated by thermogravimetric analysis (TGA, Setaram) from ambient temperature to 900 °C at a heating rate of 10 °C/min under air flow at an airflow rate of 2.5 L/min.

The crystallinity of each sample was determined by X-ray diffraction (XRD) (D8-ADVANCE powder X-ray diffractometer, Bruker, Germany), operated at 40 kV voltage and 30 mA using Ni-filtered Cu K radiation (λ = 0.15406 nm). The sample was scanned under ambient conditions over scattering 2θ from 10 to 70° with a scan rate of 0.03°/0.7 s. The crystallinity index (CrI) was calculated using Segal's method[48] following the formula:

$$\mathrm{CrI} = \frac{I_{200} - I_{\mathrm{AM}}}{I_{200}} \qquad ((1))$$

where I_{200} is the peak intensity in the plane (200) characterized for the crystallinity domain peaked at a 2θ of ∼22.8°, while I_{am} is the peak intensity in the (101) plane observed at a 2θ of ∼18° characterized for the amorphous domain in cellulose.

Particle Size and Zeta Potential Measurement. The particle size distribution and zeta potential of each sample were analyzed by a Nano-ZS analyzer (Malvern Instrument). CN suspensions (0.05 wt %) were homogenized for 10 min using Vibra Cell MC VCX750 Ultrasonic Processors at 325 W (on/off, 30/15 s). Each sample was measured 3 times, and the value of the zeta potential was estimated on average.

Quantifying the −COOH Content. The content of the functional group −COOH was quantified using an electrical conductivity method that was adapted from the Canadian Standards Association (CSA), a suggested protocol for the determination of the physical and chemical properties of CNMs entitled Cellulosic Nanomaterials—Test Methods for Characterization (CSA Z5100-14). A freeze-dried sample (0.25 g) was suspended in 100 mL of deionized water. Before titration, 250 μL of 0.1% NaCl (w/v) was added to increase the conductivity. Conductimetric titration was performed with 0.1 M NaOH as a titrant. The −COOH content was then quantified using the following equation:

$$-\mathrm{COOH\ content} = \frac{C(V_1 - V_2)}{W}(\mathrm{mmol/g}) \qquad ((2))$$

where V_2 and V_1 are the volumes of 0.1 N NaOH required to neutralize the carboxylic groups, C is the NaOH concentration (mol/L), and W is the freeze-dried sample weight. Each experiment was repeated three times, and the value of the −COOH content was averaged.

X-ray Photoemission Spectroscopy. XPS measurements were performed on a PHI Versa Probe III XPS system (ULVAC-PHI) using a monochromatic Al−K X-ray source (1486.6 eV). The base pressure was approximately 5.0×10^{-8} Pa. During the XPS measurement, the pressure was approximately 1.0×10^{-6} Pa. The samples were mounted on an XPS sample holder by using a double-sided conducting carbon adhesive tape. The X-ray spot size (diameter) was 100 μm and the source power was 25 W at 15 kV. High-resolution C_{1s} spectra were then collected.

Atomic Force Microscopy (AFM). AFM was performed by the Asylum research MFP-3D origin at an ambient temperature in contact mode with a scan rate of 1 Hz using a silicon nitride tip (Bruker DNP-10). AFM images were obtained in several size scans applying a soft force (∼1 nN) on the AFP tip, and then all data were analyzed using Gwyddion 2.59 software.

Field-Emission Scanning Electron Microscopy (FE-SEM). The nanocellulose solution was spin-coated on an SiO_2(100) wafer, and then the wafer sample was dried at 40 °C under vacuum overnight. The sample was then coated with 15 nm Ti by an e-beam evaporator (Lesker PVD-75) at 10^{-6} Torr vacuum and a depositing rate of 0.2 $nm{\cdot}s^{-1}$. The sample was then imaged by FE-SEM (JEOL, JSM-IT800) at a few kilovolts.

Cu(II) Adsorption. The adsorption of Cu(II) of bleached DFF and two CN samples was investigated by immersing 100 mg of the freeze-dried sample in 200 mL of Cu(II) 500 mg/L salt solutions. The Cu(II) concentration in the solution was then monitored by ultraviolet spectroscopy. Experiments were performed at a fixed pH of ∼4 (to avoid any possible precipitation of Cu(II)) and ambient temperature. The Cu(II) adsorption capacity of the samples was calculated according to the following equation:

$$Q_t = \frac{(C_o - C_t) \times V}{m} \qquad ((3))$$

where Q_t is the amount of adsorbed Cu(II) (mg/g), C_o (mg/L) and C_t (mg/L), respectively, are the Cu(II) concentrations before and after adsorption at a certain time, t (min), V (L) is the volume of the solution, and m (g) is the mass of the sample studied. In addition to the ultraviolet spectroscopy method, we also used atomic absorption spectroscopy to confirm Cu(II) adsorption. The obtained data were analyzed by the nonlinear pseudo-first-order and pseudo-second-order models. These two models offer information about the mechanism and interaction between the absorbate and absorbent. Generally, the first-order model implies that there is no absorbate−absorbate interaction and no difference in the interaction of absorbate and adsorption sites over the sample, which favors the physisorption process. Meanwhile, in the second-order model, the absorbate−absorbate interaction is considered, and there are energy differences between the absorbate and adsorption sites, which favor chemisorption. Isotherm experiments were carried out under ambient conditions, around pH 4.0, with the initial Cu(II) concentration adjusted from 50 to 1000 mg/L. The isotherm data were further analyzed using the Langmuir and Freundlich models, as described in the Supporting Information (SI), Sections S1 and S2.

https://doi.org/10.1021/acsomega.4c11464
ACS Omega 2025, 10, 6234−6243

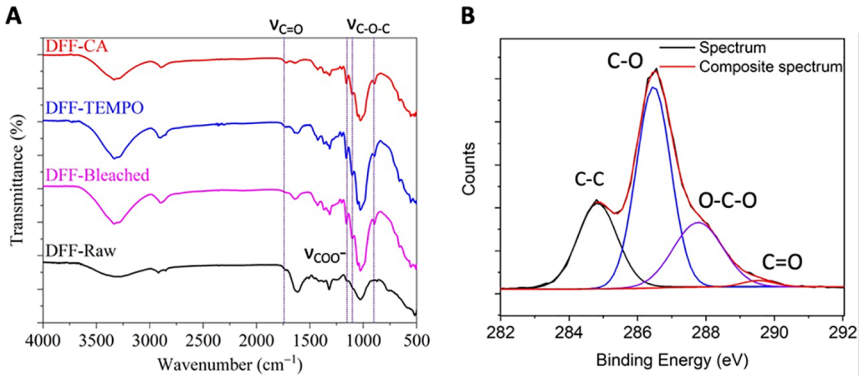

Figure 2. (A). FT-IR spectra of raw DFF (black), bleached DFF (pink), DFF-TEMPO (blue), and DFF-CA (red). (B) High-resolution C_{1s} XPS spectra of the DFF-CA sample with fitting components.

RESULTS AND DISCUSSION

Chemical Structure and Crystallinity. The components of agricultural waste DFF have previously been quantified to contain cellulose (~31%), lignin (14%), hemicellulose (~28%), and extractive and ash components (15 and 12%, respectively). The lignin, hemicellulose, and mineral contents in the bleached DFF were significantly removed and undetected by XRD.[45] The bleached DFF was then treated with TEMPO and a mixture of citric acid and HCl to produce nanocellulose.

The chemical structures of CNs isolated from DFF using TEMPO and citric acid (CA) methods are compared with the raw DFF and bleached cellulose, as presented in Figure 2A. There are vibrational bands between 899 and 1163 cm^{-1}, which are usually attributed to β-(1−4) glycosidic ether links, and the β-glycosidic linkages, C−O−C glycosidic stretching, C−OH stretching vibration, and C−O stretching, indicating the presence of a cellulose structure.[48] These bands at 1426 and 1315 cm^{-1} can be assigned to the $-CH_2-$ symmetric bending groups of cellulose. The band at 1641 cm^{-1} existed in all samples and could be assigned to the vibrational binding of water molecules adsorbed onto cellulose. In the spectra of raw DFF, there are vibrational bands at 1514 and 1460 cm^{-1} due to the stretching vibrations of the C=C and C=C−C groups of the lignin component; however, these bands almost disappeared in the spectra of the bleached cellulose and all CNs. This observation indicated the removal of lignin in bleached cellulose and CN samples, and, more importantly, the chemical structure of cellulose remains in all samples. The C=O vibration at 1740 cm^{-1} also appeared in the spectra of DFF-CA and DFF-TEMPO, and the vibrational band peak at 1242 cm^{-1} is assigned to the symmetrical vibration of the COO^- group, which could be explained by the existence of the COOH group functionalized on nanocellulose. Interestingly, the vibrational band peaked at 1740 cm^{-1} in the raw DFF sample is usually assigned to the vibration of the C=O chemical group in lignin; however, vibration still existed in the bleached DFF, which could be generated during the bleaching process using oxidative chemical compounds; we note here that the process is usually repeated 4 times. To qualitatively estimate the C=O content in these samples, we normalized the C=O vibrational peak at 1740 cm^{-1} to the peak at 1163 cm^{-1}. We observed that the C=O content in DFF-CA is higher than that in the DFF-TEMPO and bleached DFF samples. In summary, the FT-IR data indicated the removal of lignin and hemicellulose, while the chemical structure of cellulose remained unchanged; however, there is an appearance of the COOH group on the bleached DFF, DFF-CA, and DFF-TEMPO samples.

XPS was then used to analyze the presence of the −COOH group on the surfaces of the DFF-CA sample by deconvoluted high-resolution C_{1s} spectra (see Figure 2B). The deconvolution used Gaussian peak shapes and integrated background subtraction, and for the fits, the peak positions were fixed according to tabulated chemical shifts and guidelines established.[48] We note that ideal cellulose is devoid of the C−C components of the C 1s signal at 284.8 eV because of its polysaccharide structure; however, in our samples, the C−C component of approximately 10% of total carbon was obtained. The result indicates an extraordinarily low level of adventitious contamination in DFF-CA, hemicelluloses, or lignin residues if the remaining C−C level is due to hydrocarbons absorbed in DFF-CA samples. More importantly, we observed the existence of a C=O carboxylic peak at 289.6 eV, an O−C−O peak at 288 eV, and a C−O peak at 286.7 eV, providing evidence of carboxylic groups functionalizing DFF-CA samples.[49] The signal of the −COOH group was further evidenced by the FT-IR spectra, as shown in Figure S1. Briefly, the dried DFF-CA sample was immersed in NaOH 0.5 M for 15 min, then rinsed with NaOH, and then dried in the oven for 3 h. Figure S1 compared the spectra of the DFF-CA and NaOH-treated DFF-CA samples, and as shown, there is a new vibrational frequency peaked at 1465 cm^{-1}, which can be assigned to the asymmetrical vibration of the $-COO^-$ group.

The crystalline structure and crystallinity of all samples were determined by XRD analysis, and the data are presented in Figure 3. All samples show the signature of the cellulose I structure as expected for natural cellulosic materials, which is usually characterized by the diffraction peaks at 14−17°, 22.3°, and 34° corresponding to (110), (101), (200), and (400).[48,50] Importantly, we observed that the intensity of these peaks in bleached DFF, especially CNs, is greater than that of raw DFF, which suggests the removal of most amorphous/crystal noncellulosic components, lignin, and hemicellulose. The DFF-CA spectra presented the narrowest and sharpest pattern, especially at a 2θ of ~22.3° and an additional pattern that peaked at a 2θ of ~34° assigned to the (400) plane. The crystallinity index (CrI) of all samples was quantified by Segal's method (eq (1)). The CrI of the raw DFF was 52.5%, and the CrI of the bleached DFF increased to 63.9% due to the removal of hemicellulose and lignin. The CrI values of the DFF-TEMPO and DFF-CA samples were approximately 61.8

https://doi.org/10.1021/acsomega.4c11464
ACS Omega 2025, 10, 6234−6243

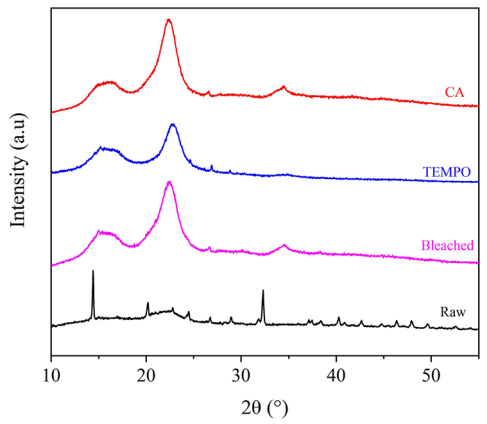

Figure 3. XRD patterns of raw DFF (black), bleached DFF (pink), DFF-TEMPO (blue), and DFF-CA (red) samples.

and 74.6%, respectively, which is greater than that of raw DFF, and its value is also consistent with the cellulose nanomaterial isolated by both the TEMPO and citric acid methods.[51−53] Here, the XRD results demonstrated that (i) the stability of the cellulose I structure before and after bleaching treatment and hydrolysis with acid citric and (ii) the removal of lignin, hemicellulose, and other components led to greater CrI, especially in DFF-CA and DFF-TEMPO.

Thermal Stability of CNs. The thermal stability of DFF-TEMPO and DFF-CA evaluated by TGA/DTG analysis in the range of 70−880 °C is presented in Figure 4. As expected for lignocellulosic materials, the decomposition of CNs occurred in 3 steps, as shown in Figure 4. The initial step of degradation occurred at a T_{onset} of ∼110 °C, which could be assigned to the weight loss (10%) due to loss of moisture in all lignocellulose samples. The second step is the degradation stage occurring from 250 to 450 °C, where the crystalline region started to decompose with significant weight loss (∼80%) due to the gas phase transition and tar formation. The T_{onset} of the second step, ∼250 °C for DFF-TEMPO and DFF-CA, respectively, is also slightly higher than that of CN generated from the hydrolysis of the H_2SO_4-catalyzed cellulosic material that was obtained from our previous report, labeled DFF-H_2SO_4.[45] During the last stage, in the range of 450−600 °C, the cellulosic crystalline structure was completely decomposed into volatiles and tar. We also note that the tar concentration in the DFF-CA sample is only 4%, which is slightly lower than that in the bleached and raw samples, indicating the removal of mineral and lignin components.

Dimension and Surface of CNs. Dynamic light scattering (DLS) was first performed to estimate the size distribution profile of the cellulose nanomaterials in a colloidal suspension. Figure 5A shows the size distributions obtained for the DFF-TEMPO and DFF-CA samples. It shows the particle size distribution of the DFF-CA sample ranging from 120 to 350 nm, with an average particle size of 220 ± 50 nm, while the PSD of DFF-TEMPO prepared by the TEMPO agent ranged from 400 to 800 nm, with an average particle size of 600 ± 100 nm. In general, the DLS results show that the average size of DFF-CA is much smaller than that of DFF-TEMPO, which is expected, as the TEMPO agent is known to form cellulose nanomaterials in the form of fibers (as also shown in Figure S2), whereas the mixture of citric acid and HCl forms a rod-like shape.[47,52] The dimensions of DFF-CA were further confirmed by AFM measurements, as shown in Figure 5B for the DFF-CA sample. A droplet of diluted CN suspensions (∼0.01 wt %) was first deposited on a fresh SiO_2 substrate (2 × 2 cm^2), and the sample was then dried at ambient temperature. Figure 5B reveals the rod-shaped appearance of the DFF-CA sample with width in the range of 200−400 nm and a height of 2−10 nm, which agrees well with the DLS results. To further confirm the rod shape of DFF-CA, we performed SEM observations, as shown in Figure 5C. Our dimension analysis confirmed that DFF-CA nanocrystals are rod-shaped with a diameter of approximately 360 nm.

Zeta potential analysis was performed to measure the surface charge of the nanoparticle. The value of electrical charges commonly measured in millivolts (mV) will define the stability of a nanoparticle in a colloidal suspension. In general, a potential zeta value of <−30 and >30 mV was considered to be adequate repulsive force to achieve a stable colloidal suspension. In fact, we observed that the zeta potentials of DFF-CA and DFF-TEMPO were −64.6 and −40.7 mV, respectively. This negative value was due to the electrostatic repulsion between the nanoparticles with the same electric charge, preventing agglomeration, as shown in Figure 1. Moreover, this large negative zeta potential indicates the existence of negatively charged functional groups on the

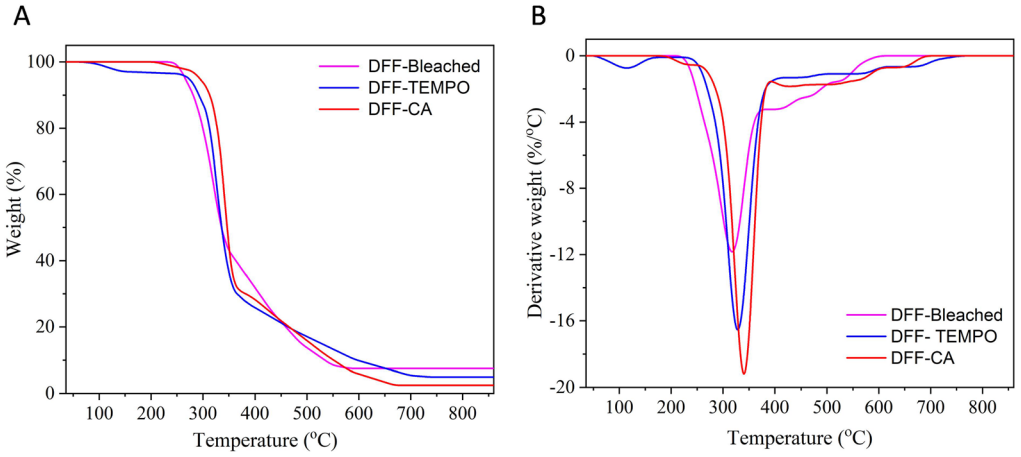

Figure 4. Thermal analysis of the bleached DFF, DFF-TEMPO, and DFF-CA samples: (A) TGA and (B) DTG. The results show significant weight loss in a range of 250−450 °C, approximately 80%.

https://doi.org/10.1021/acsomega.4c11464
ACS Omega 2025, 10, 6234−6243

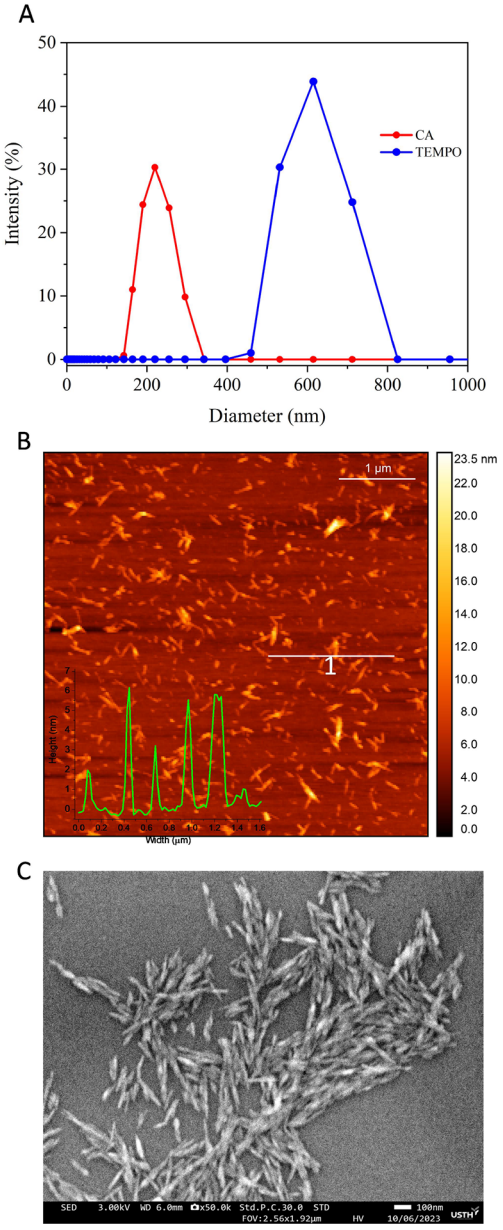

Figure 5. (A) Particle size distribution of DFF-CA and DFF-TEMPO obtained from DLS measurements. (B) AFM image of DFF-CA with the inset showing the height profile taken from line 1. (C) SEM micrograph of isolated DFF-CA.

surface of the CNs, which could be assigned to the carboxylic, −COOH, group. To quantify the −COOH content, we then used the conductometric titration method, which has been used previously, and the result is shown in Figure S3 and summarized in Table 1. As shown, the −COOH content of the DFF-CA and DFF-TEMPO samples is a few times greater than that of the bleached sample and DFF-H_2SO_4, which probably resulted in a lower zeta potential.

Cu(II) Adsorption. *Kinetics of Cu(II) Adsorption by the DFF-CA Sample.* To understand the kinetic mechanism for the removal of Cu (II) of the carboxylate cellulose nanomaterial, we evaluated the removal capacity (Q_t) versus contact time (t) in the range of 0−300 min as presented in Figure 6. As shown, the removal efficiency increases rapidly at the beginning of the experiment and then reaches equilibrium after 10 min (Figure 6A), indicating an equilibrium removal capacity (Q_e) of approximately 227 mg·g^{-1}.

Both the Lagergren pseudo-first-order and Lagergren pseudo-second-order models (more details in SI, Sections S1 and S2) were utilized to exploit the kinetics of Cu (II) removal, and the fitting results based on experimental data are shown in Figure 6B,C. The linear correlation coefficient (R^2) values for pseudo-first-order and pseudo-second-order models are 0.17 and 0.99, respectively. These fitting results show that the DFF-CA kinetics for Cu(II) removal can be explained by the Lagergren pseudo-second-order kinetic model, which means that Cu(II) removal by CNs-CA occurred by a chemisorption process.

Isotherm of Cu(II) Adsorption by DFF-CA. Next, we attempted to investigate the relationship between the initial Cu concentration (II) and equilibrium removal capacity of the DFF-CA sample, as shown in Figure 7A, and then the results were fitted with the Langmuir and Freundlich adsorption isotherm models, as presented in Figure 7B,C. The experimental data in Figure 7B were fitted with the Langmuir model, which has a linear R^2 of 0.95, while a linear R^2 of 0.53 was obtained from the fitting based on the Freundlich model. These results suggest that the adsorption of Cu(II) by DFF-CA is a monolayer process over a homogeneous DFF-CA surface with identical and energetically equivalent active sites.

The Langmuir adsorption model was then used to estimate the maximum removal capacity of the CNs-CA sample for Cu(II), which shows a value of 227 mg·g^{-1}. In our case, the as-prepared DFF-CA sample exhibited an excellent Cu(II) removal performance compared to the previous report and was better than many other nanomaterial adsorbents such as modified TiO_2, carbon nanotubes, and activated granular carbon.[54−56]

Recently, Liu et al. reported that CNs with a carboxylate content of 1.5 mmol·g^{-1} produced by TEMPO oxidation had a maximum Cu(II) adsorption capacity of 75 mg·g^{-1}.[51] Famei et al. then reported the maximum Cu(II) adsorption capacity (∼115.3 mg·g^{-1}) of cellulose nanofibrils and attributed this to the high −COOH concentration of 2.7 mmol·g^{-1}.[35] Sehaqui et al. also reported that by optimizing the pH and surface of CN, the maximum Cu(II) capacity of the TEMPO-oxidation CNs was 135 mg·g^{-1}, and importantly, the adsorbent can be easily regenerated by acid washing.[57] On the other hand, Kardam et al. reported the low adsorption capacity (<20 mg·g^{-1}) of native cellulose nanofibrils, which was assigned to the low affinity of

Table 1. Summaries of Physical Parameters Obtained for Bleached DFF, DFF-H_2SO_4, DFF-TEMPO, and DFF-CA Samples

sample	−COOH content (mmol/g cellulose)	zeta potential (mV)	size diameter (nm)	crystallinity (%)
DFF-bleached	0.3587 ± 0.0279	−36.90 ± 6.95		63.9
DFF-H_2SO_4	0.7365 ± 0.0118	−49.70 ± 1.27	312.9 ± 14.23	84.8
DFF-TEMPO	1.7045 ± 0.1054	−64.60 ± 1.57	468.2 ± 50.95	61.8
DFF-CA	1.2948 ± 0.0072	−40.70 ± 0.75	362.2 ± 21.75	74.6

https://doi.org/10.1021/acsomega.4c11464
ACS Omega 2025, 10, 6234−6243

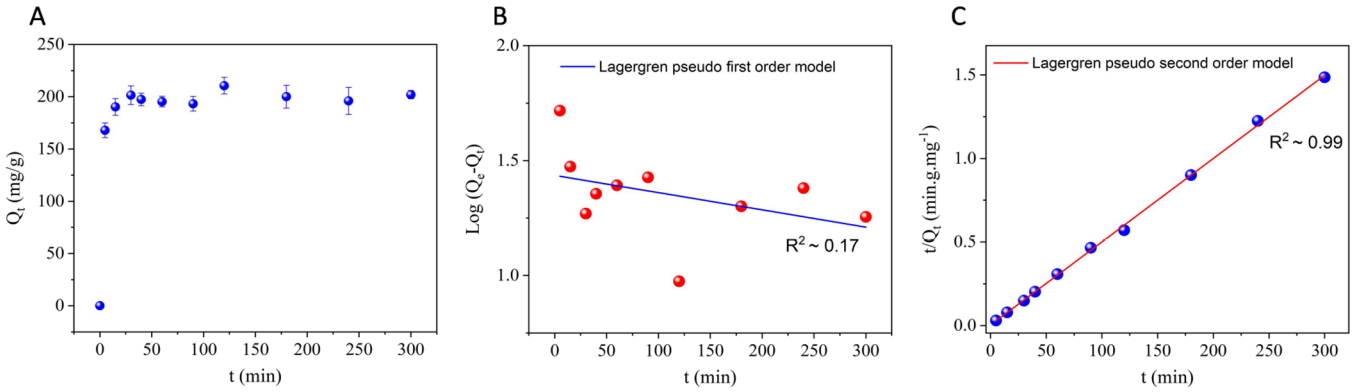

Figure 6. (A) Contact time versus removal capacity of DFF-CA for Cu^{2+}. Kinetics model of DFF-CA for Cu^{2+} removal: (B) Lagergren pseudo-first-order and (C) Lagergren pseudo-second-order models.

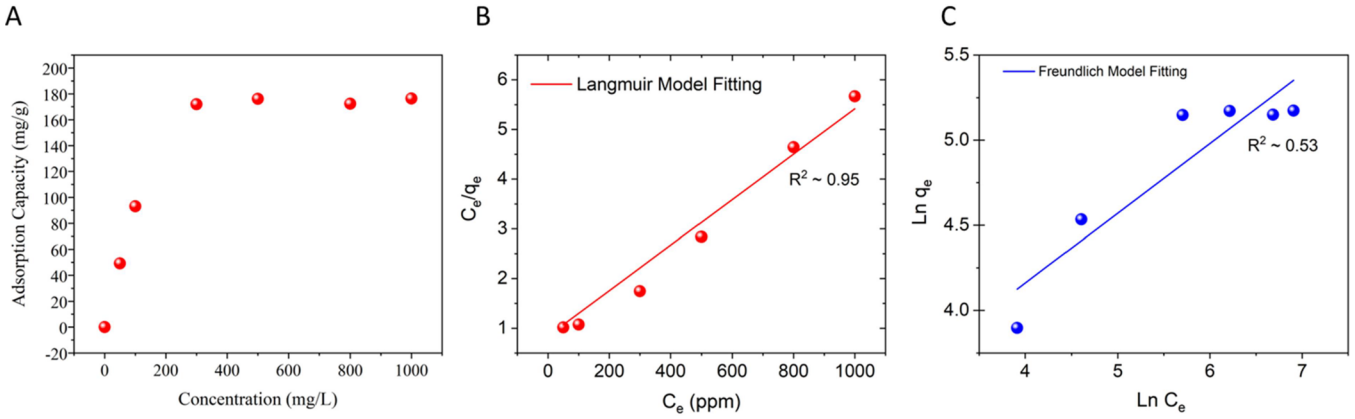

Figure 7. (A) Initial Cu (II) concentrations versus the removal capacity of DFF-CA. Data fitted with (B) the Langmuir and (C) Freundich adsorption isotherm models.

hydroxyl, −OH, groups.[58] Its enhanced performance was widely agreed upon to be caused by the strong affinity of the carboxylate groups on the surface of CNs. However, using XPS, Magallanes et al. recently reported that the affinities of carboxylate and hydroxyl group toward Cu^{2+} were similar.[44]

To further understand the effect of the −COOH content, we first quantified the −COOH content of several samples including DFF-bleached, DFF-H_2SO_4, DFF-CA, and DFF-TEMPO samples and then investigated the relation between the −COOH content and Cu^{2+} adsorption. The Cu^{2+} maximum adsorption for each sample was plotted, as shown in Figure S4. Figure 8 displays the relationship of the −COOH content and Cu^{2+} adsorption capacity with the standard deviation. Interestingly, we observed that the Cu^{2+} maximum adsorption was almost similar, even though the −COOH content varied 5 times from DFF-bleached to DFF-TEMPO samples. To determine the accuracy of our Cu^{2+} quantitative analysis, we performed atomic adsorption spectrophotometry to quantify the Cu^{2+} content; however, we did not observe a clear difference between both methods. Like the effect of the −COOH content, we also observed that the Cu^{2+} adsorption is almost independent of the negative zeta potential. We also neglect the effect of surface area on the Cu^{2+} adsorption since the particle size of DFF-CA and DFF-TEMPO are much smaller (~200 times) than that of the bleached sample, but the adsorption capacity changed only by 1.2 times. Our result showed that the affinity of Cu^{2+} toward the −COOH and −OH groups was strong, fast, and almost similar. Our results

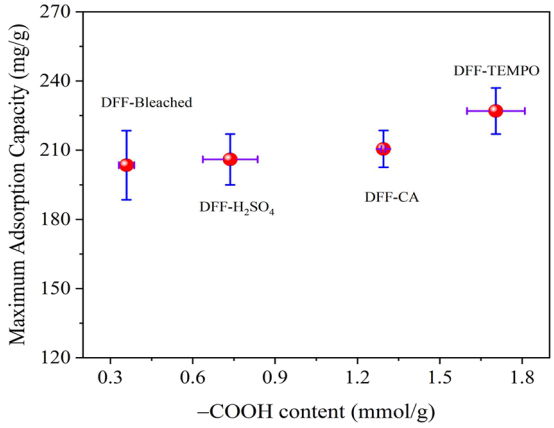

Figure 8. Plot presenting the relationship between the content of −COOH group and the maximum Cu(II) adsorption capacity.

could be explained by the fact that in an acid solution, the Cu^{2+} ion was solvated and formed the hydrated state such as $[Cu(H_2O)_n]^{2+}$, where n could be in the range of 3−8.[59,60] As a result, the Cu^{2+} ion was not in direct contact with the −COOH or −OH group; instead, the hydrated state was in direct contact with the −COOH or −OH group; then, the interaction force including hydrogen bonding or electrostatic force between $[Cu(H_2O)_n]^{2+}\cdots$OH or $[Cu(H_2O)_n]^{2+}\cdots$COOH was almost similar. Further experiments such as deuterium labeling the −COOH group, or heavy water D_2O, and

https://doi.org/10.1021/acsomega.4c11464
ACS Omega 2025, 10, 6234−6243

advanced quantum chemical calculations are necessary to better understand the interaction force.

To investigate the antimicrobial properties of the Cu-containing cellulose gel, we first prepared a cellulose gel based on a previous report,[61] then adsorbed Cu^{2+} into the cellulose gel, as shown in Figure S5, and finally, the gel was placed in glycerol and used for the antimicrobial test. We then examined the inhibition zones of gels against specific bacteria strains (*L. monocytogenes* ATCC 35152, *B. cereus* ATCC 147337, *S. typhimurium* ATCC 13311, *E. coli* ATCC 11105, and *V. parahemolyticus*), which were measured and recorded, as shown in Figure S6 and Table S1. To establish a benchmark, an antibiotic ampicillin (at 50 mg/mL) was added to compare bacterial growth inhibition between the different gels. Our primary findings indicated that the copper-containing cellulose gel demonstrated great antibacterial activity; however, further optimization of the Cu-containing cellulose gel and the mechanism of the antimicrobial require a deeper investigation.

CONCLUSIONS

In summary, we successfully extracted CNs functionalized with the −COOH group from the agricultural waste DFF. The COOH-functionalized CNs were then characterized by FT-IR spectroscopy and XRD, suggesting the removal of the lignin and hemicellulose contents, while the signals for cellulose contents remain the same for DFF-CA and DFF-TEMPO. The DLS, AFM, and SEM results indicated that the DFF-CA sample has a smaller average particle size (220 ± 50 nm) compared to the DFF-TEMPO sample (600 ± 100 nm). DFF-CA particles exhibit a rod-like shape, while DFF-TEMPO particles are larger and fiber-shaped. Importantly, the CNs extracted from DFF, including bleached DFF, DFF-TEMPO, and DFF-CA, exhibited promising properties for Cu(II) adsorption, with a maximum adsorption of 227 $mg{\cdot}g^{-1}$, and the Cu^{2+} adsorption is almost independent of the −COOH content. Our result showed that the Cu^{2+} affinity of −COOH and −OH groups was almost similar, and more importantly, the Cu-containing cellulose gel can be used in antimicrobial applications. In general, our work opens new possibilities for the use of unexplored cellulosic byproducts in the agricultural industry as well as potential application of Cu- containing cellulose gel as an antimicrobial.

ASSOCIATED CONTENT

Supporting Information

The Supporting Information is available free of charge at https://pubs.acs.org/doi/10.1021/acsomega.4c11464.

FT-IR spectra, SEM images, titration method, antimicrobial activity, and kinetic and isotherm models (PDF)

AUTHOR INFORMATION

Corresponding Author

Quyen Van Nguyen − *Department of Advanced Materials Science and Nanotechnology, University of Science and Technology of Hanoi (USTH), Vietnam Academy of Science and Technology, 11307 Hanoi, Vietnam;* orcid.org/0000-0003-0120-0971; Email: nguyen-van.quyen@usth.edu.vn

Authors

Thai Anh Do − *Department of Advanced Materials Science and Nanotechnology, University of Science and Technology of Hanoi (USTH), Vietnam Academy of Science and Technology, 11307 Hanoi, Vietnam*

Anh Tuyet Phung Thi − *Institute of Chemistry, Vietnam Academy of Science and Technology, 11307 Hanoi, Vietnam*

Thi Huong Le − *Department of Advanced Materials Science and Nanotechnology, University of Science and Technology of Hanoi (USTH), Vietnam Academy of Science and Technology, 11307 Hanoi, Vietnam*

Dang Do Van − *Faculty of Chemistry, University of Science, 11021 Hanoi, Vietnam*

Thoa Nguyen Kim − *Institute of Biotechnology, Vietnam Academy of Science and Technology, 11307 Hanoi, Vietnam*

Complete contact information is available at: https://pubs.acs.org/10.1021/acsomega.4c11464

Author Contributions

This manuscript was written with the contributions of all authors. All authors have approved the final version of the manuscript. T.A.D., A.T.P.T., and Q.V.N.: equally contribution.

Notes

The authors declare no competing financial interest.

ACKNOWLEDGMENTS

The author acknowledges the Vietnam Academy of Science and Technology for its financial support (TĐNSH0.03/22-24). The author thanks Dr. Bing Lu at the Characterization Facility at the College of Science and Engineering at the University of Minnesota for his support with XPS.

REFERENCES

(1) Moon, R. J.; Martini, A.; Nairn, J.; Simonsen, J.; Youngblood, J. Cellulose Nanomaterials Review: Structure, Properties and Nanocomposites. *Chem. Soc. Rev.* **2011**, *40* (7), 3941−3994.

(2) Li, T.; Chen, C.; Brozena, A. H.; Zhu, J. Y.; Xu, L.; Driemeier, C.; Dai, J.; Rojas, O. J.; Isogai, A.; Wågberg, L.; Hu, L.; et al. *Nature* **2021**, *590* (7844), 47−56.

(3) Chen, W.; Yu, H.; Lee, S.-Y.; Wei, T.; Li, J.; Fan, Z. Nanocellulose: A Promising Nanomaterial for Advanced Electrochemical Energy Storage. *Chem. Soc. Rev.* **2018**, *47* (8), 2837−2872.

(4) Jorfi, M.; Foster, E. J. Recent Advances in Nanocellulose for Biomedical Applications. *J. Appl. Polym. Sci.* **2015**, *132* (14), 41719.

(5) Yang, X.; Biswas, S. K.; Han, J.; Tanpichai, S.; Li, M.; Chen, C.; Zhu, S.; Das, A. K.; Yano, H. Surface and Interface Engineering for Nanocellulosic Advanced Materials. *Adv. Mater.* **2021**, *33* (28), No. 2002264.

(6) Heise, K.; Kontturi, E.; Allahverdiyeva, Y.; Tammelin, T.; Linder, M. B.; Nonappa; Ikkala, O. Nanocellulose: Recent Fundamental Advances and Emerging Biological and Biomimicking Applications. *Adv. Mater.* **2021**, *33* (3), No. 2004349.

(7) Habibi, Y.; Lucia, L. A.; Rojas, O. J. Cellulose Nanocrystals: Chemistry, Self-Assembly, and Applications. *Chem. Rev.* **2010**, *110* (6), 3479−3500.

(8) Han, C.; Cao, M.; Yu, J.; Wang, S.; Zhou, X.; Chen, Y.; Yang, F. Carboxymethyl Cellulose-Based Composite Polymer Hydrogels Cross-Linked with Epichlorohydrin and Application for Cu(II) Removal. *ACS Appl. Polym. Mater.* **2023**, *5* (3), 2070−2078.

(9) Kaur, J.; Sengupta, P.; Mukhopadhyay, S. Critical Review of Bioadsorption on Modified Cellulose and Removal of Divalent Heavy Metals (Cd, Pb, and Cu). *Ind. Eng. Chem. Res.* **2022**, *61* (5), 1921−1954.

(10) Zhu, H.; Luo, W.; Ciesielski, P. N.; Fang, Z.; Zhu, J. Y.; Henriksson, G.; Himmel, M. E.; Hu, L. Wood-Derived Materials for Green Electronics, Biological Devices, and Energy Applications. *Chem. Rev.* **2016**, *116* (16), 9305−9374.

(11) Yu, H.-Y.; Zhang, H.; Song, M.-L.; Zhou, Y.; Yao, J.; Ni, Q.-Q. From Cellulose Nanospheres, Nanorods to Nanofibers: Various Aspect Ratio Induced Nucleation/Reinforcing Effects on Polylactic Acid for Robust-Barrier Food Packaging. *ACS Appl. Mater. Interfaces* **2017**, *9* (50), 43920−43938.
(12) Dong, X. M.; Revol, J. F.; Gray, D. G. Effect of Microcrystallite Preparation Conditions on the Formation of Colloid Crystals of Cellulose. *Cellulose* **1998**, *5* (1), 19−32.
(13) Yu, H.; Qin, Z.; Liang, B.; Liu, N.; Zhou, Z.; Chen, L. Facile Extraction of Thermally Stable Cellulose Nanocrystals with a High Yield of 93% through Hydrochloric Acid Hydrolysis under Hydrothermal Conditions. *J. Mater. Chem. A* **2013**, *1* (12), 3938−3944.
(14) Feese, E.; Sadeghifar, H.; Gracz, H. S.; Argyropoulos, D. S.; Ghiladi, R. A. Photobactericidal Porphyrin-Cellulose Nanocrystals: Synthesis, Characterization, and Antimicrobial Properties. *Biomacromolecules* **2011**, *12* (10), 3528−3539.
(15) Du, H.; Parit, M.; Wu, M.; Che, X.; Wang, Y.; Zhang, M.; Wang, R.; Zhang, X.; Jiang, Z.; Li, B. Sustainable Valorization of Paper Mill Sludge into Cellulose Nanofibrils and Cellulose Nanopaper. *J. Hazard Mater.* **2020**, *400*, No. 123106.
(16) Tang, L.; Huang, B.; Lu, Q.; Wang, S.; Ou, W.; Lin, W.; Chen, X. Ultrasonication-Assisted Manufacture of Cellulose Nanocrystals Esterified with Acetic Acid. *Bioresour. Technol.* **2013**, *127*, 100−105.
(17) Galland, S.; Berthold, F.; Prakobna, K.; Berglund, L. A. Holocellulose Nanofibers of High Molar Mass and Small Diameter for High-Strength Nanopaper. *Biomacromolecules* **2015**, *16* (8), 2427−2435.
(18) Man, Z.; Muhammad, N.; Sarwono, A.; Bustam, M. A.; Kumar, M. V.; Rafiq, S. Preparation of Cellulose Nanocrystals Using an Ionic Liquid. *J. Polym. Environ.* **2011**, *19* (3), 726−731.
(19) Han, J.; Zhou, C.; French, A. D.; Han, G.; Wu, Q. Characterization of Cellulose II Nanoparticles Regenerated from 1-Butyl-3-Methylimidazolium Chloride. *Carbohydr. Polym.* **2013**, *94* (2), 773−781.
(20) Lazko, J.; Sénéchal, T.; Landercy, N.; Dangreau, L.; Raquez, J. M.; Dubois, P. Well Defined Thermostable Cellulose Nanocrystals via Two-Step Ionic Liquid Swelling-Hydrolysis Extraction. *Cellulose* **2014**, *21* (6), 4195−4207.
(21) Ashori, A.; Babaee, M.; Jonoobi, M.; Hamzeh, Y. Solvent-Free Acetylation of Cellulose Nanofibers for Improving Compatibility and Dispersion. *Carbohydr. Polym.* **2014**, *102*, 369−375.
(22) Beaumont, M.; Otoni, C. G.; Mattos, B. D.; Koso, T. V.; Abidnejad, R.; Zhao, B.; Kondor, A.; King, A. W. T.; Rojas, O. J. Regioselective and Water-Assisted Surface Esterification of Never-Dried Cellulose: Nanofibers with Adjustable Surface Energy. *Green Chem.* **2021**, *23* (18), 6966−6974.
(23) Bangar, S. P.; Harussani, M. M.; Ilyas, R. A.; Ashogbon, A. O.; Singh, A.; Trif, M.; Jafari, S. M. Surface Modifications of Cellulose Nanocrystals: Processes, Properties, and Applications. *Food Hydrocoll* **2022**, *130*, No. 107689.
(24) Carpenter, A. W.; de Lannoy, C.-F.; Wiesner, M. R. Cellulose Nanomaterials in Water Treatment Technologies. *Environ. Sci. Technol.* **2015**, *49* (9), 5277−5287.
(25) Abitbol, T.; Kloser, E.; Gray, D. G. Estimation of the Surface Sulfur Content of Cellulose Nanocrystals Prepared by Sulfuric Acid Hydrolysis. *Cellulose* **2013**, *20* (2), 785−794.
(26) Etale, A.; Onyianta, A. J.; Turner, S. R.; Eichhorn, S. J. Cellulose: A Review of Water Interactions, Applications in Composites, and Water Treatment. *Chem. Rev.* **2023**, *123* (5), 2016−2048.
(27) Si, R.; Pu, J.; Luo, H.; Wu, C.; Duan, G. Nanocellulose-Based Adsorbents for Heavy Metal Ion. *Polymers (Basel)* **2022**, *14* (24), 5479.
(28) Chen, C.; Hu, L. Nanocellulose toward Advanced Energy Storage Devices: Structure and Electrochemistry. *Acc. Chem. Res.* **2018**, *51* (12), 3154−3165.
(29) Li, Q.; Wei, B.; Lu, L.; Li, Y.; Wen, Y.; Pu, W.; Li, H.; Wang, C. Investigation of Physical Properties and Displacement Mechanisms of Surface-Grafted Nano-Cellulose Fluids for Enhanced Oil Recovery. *Fuel* **2017**, *207*, 352−364.
(30) Abeer, M. M.; Mohd Amin, M. C. I.; Martin, C. A Review of Bacterial Cellulose-Based Drug Delivery Systems: Their Biochemistry, Current Approaches and Future Prospects. *J. Pharm. Pharmacol.* **2014**, *66* (8), 1047−1061.
(31) Ahmad, H. Celluloses as Support Materials for Antibacterial Agents: A Review. *Cellulose* **2021**, *28* (5), 2715−2761.
(32) Hemraz, U. D.; Lam, E.; Sunasee, R. Recent Advances in Cellulose Nanocrystals-Based Antimicrobial Agents. *Carbohydr. Polym.* **2023**, *315*, No. 120987.
(33) Gómez, H. C.; Serpa, A.; Velásquez-Cock, J.; Gañán, P.; Castro, C.; Vélez, L.; Zuluaga, R. Vegetable Nanocellulose in Food Science: A Review. *Food Hydrocolloids* **2016**, *57*, 178−186.
(34) Liu, P.; Oksman, K.; Mathew, A. P. Surface Adsorption and Self-Assembly of Cu(II) Ions on TEMPO-Oxidized Cellulose Nanofibers in Aqueous Media. *J. Colloid Interface Sci.* **2016**, *464*, 175−182.
(35) Qin, F.; Fang, Z.; Zhou, J.; Sun, C.; Chen, K.; Ding, Z.; Li, G.; Qiu, X. Efficient Removal of Cu $^{2+}$ in Water by Carboxymethylated Cellulose Nanofibrils: Performance and Mechanism. *Biomacromolecules* **2019**, *20* (12), 4466−4475.
(36) Valencia, L.; Kumar, S.; Nomena, E. M.; Salazar-Alvarez, G.; Mathew, A. P. In-Situ Growth of Metal Oxide Nanoparticles on Cellulose Nanofibrils for Dye Removal and Antimicrobial Applications. *ACS Appl. Nano Mater.* **2020**, *3* (7), 7172−7181.
(37) Salah, I.; Parkin, I. P.; Allan, E. Copper as an Antimicrobial Agent: Recent Advances. *RSC Adv.* **2021**, *11* (30), 18179−18186.
(38) Yu, J.; Huang, X.; Ren, F.; Cao, H.; Yuan, M.; Ye, T.; Xu, F. Application of Antimicrobial Properties of Copper. *Appl. Organomet. Chem.* **2024**, *38* (7), No. e7506.
(39) Vincent, M.; Duval, R. E.; Hartemann, P.; Engels-Deutsch, M. Contact Killing and Antimicrobial Properties of Copper. *J. Appl. Microbiol.* **2018**, *124* (5), 1032−1046.
(40) Vincent, M.; Hartemann, P.; Engels-Deutsch, M. Antimicrobial Applications of Copper. *Int. J. Hyg Environ. Health* **2016**, *219* (7), 585−591.
(41) Sheng, P. X.; Ting, Y.-P.; Chen, J. P.; Hong, L. Sorption of Lead, Copper, Cadmium, Zinc, and Nickel by Marine Algal Biomass: Characterization of Biosorptive Capacity and Investigation of Mechanisms. *J. Colloid Interface Sci.* **2004**, *275* (1), 131−141.
(42) Song, X.; Gunawan, P.; Jiang, R.; Leong, S. S. J.; Wang, K.; Xu, R. Surface Activated Carbon Nanospheres for Fast Adsorption of Silver Ions from Aqueous Solutions. *J. Hazard Mater.* **2011**, *194*, 162−168.
(43) Yang, L.; Li, Y.; Jin, X.; Ye, Z.; Ma, X.; Wang, L.; Liu, Y. Synthesis and Characterization of a Series of Chelating Resins Containing Amino/Imino-Carboxyl Groups and Their Adsorption Behavior for Lead in Aqueous Phase. *Chemical Engineering Journal* **2011**, *168* (1), 115−124.
(44) Magallanes, C.; Aguirre, B. M.; González, G. A.; Méndez De Leo, L. P. Interaction of Aqueous Cu(II) with Carboxylic Acid and Alcohol Terminated Self Assembled Monolayers: Surface and Interfacial Characterization. *Surf. Sci.* **2020**, *692*, No. 121529.
(45) Anh, T. P. T.; Nguyen, T. V.; Hoang, P. T.; Thi, P. V.; Kim, T. N.; Van, Q. N.; Van, C. N.; Hai, Y. D. Dragon Fruit Foliage: An Agricultural Cellulosic Source to Extract Cellulose Nanomaterials. *Molecules* **2021**, *26* (24), 7701.
(46) Hassan, S. H.; Velayutham, T. S.; Chen, Y. W.; Lee, H. V. TEMPO-Oxidized Nanocellulose Films Derived from Coconut Residues: Physicochemical, Mechanical and Electrical Properties. *Int. J. Biol. Macromol.* **2021**, *180*, 392−402.
(47) Isogai, A.; Saito, T.; Fukuzumi, H. TEMPO-Oxidized Cellulose Nanofibers. *Nanoscale* **2011**, *3* (1), 71−85.
(48) Foster, E. J.; Moon, R. J.; Agarwal, U. P.; Bortner, M. J.; Bras, J.; Camarero-Espinosa, S.; Chan, K. J.; Clift, M. J. D.; Cranston, E. D.; Eichhorn, S. J.; Fox, D. M.; Hamad, W. Y.; Heux, L.; Jean, B.; Korey, M.; Nieh, W.; Ong, K. J.; Reid, M. S.; Renneckar, S.; Roberts, R.; Shatkin, J. A.; Simonsen, J.; Stinson-Bagby, K.; Wanasekara, N.;

https://doi.org/10.1021/acsomega.4c11464
ACS Omega 2025, 10, 6234−6243

Youngblood, J. Current Characterization Methods for Cellulose Nanomaterials. *Chem. Soc. Rev.* **2018**, *47* (8), 2609−2679.
(49) Johansson, L. S.; Campbell, J. M.; Koljonen, K.; Stenius, P. Evaluation of Surface Lignin on Cellulose Fibers with XPS. *Appl. Surf. Sci.* **1999**, *144*−*145*, 92−95.
(50) Nam, S.; French, A. D.; Condon, B. D.; Concha, M. Segal Crystallinity Index Revisited by the Simulation of X-Ray Diffraction Patterns of Cotton Cellulose Iβ and Cellulose II. *Carbohydr. Polym.* **2016**, *135*, 1−9.
(51) Liu, S.; Low, Z.; Xie, Z.; Wang, H. TEMPO-Oxidized Cellulose Nanofibers: A Renewable Nanomaterial for Environmental and Energy Applications. *Adv. Mater. Technol.* **2021**, *6* (7), No. 2001180.
(52) Bondancia, T. J.; de Aguiar, J.; Batista, G.; Cruz, A. J. G.; Marconcini, J. M.; Mattoso, L. H. C.; Farinas, C. S. Production of Nanocellulose Using Citric Acid in a Biorefinery Concept: Effect of the Hydrolysis Reaction Time and Techno-Economic Analysis. *Ind. Eng. Chem. Res.* **2020**, *59* (25), 11505−11516.
(53) Nasihin, Z. D.; Masruri, M.; Warsito, W.; Srihardyastutie, A. Preparation of Nanocellulose Bioplastic with a Gradation Color of Red and Yellow. *IOP Conf Ser. Mater. Sci. Eng.* **2020**, *833* (1), No. 012078.
(54) Su, C.; Berekute, A. K.; Yu, K.-P. Chitosan@TiO2 Composites for the Adsorption of Copper(II) and Antibacterial Applications. *Sustainable Environment Research* **2022**, *32* (1), 27.
(55) Gupta, V. K.; Agarwal, S.; Bharti, A. K.; Sadegh, H. Adsorption Mechanism of Functionalized Multi-Walled Carbon Nanotubes for Advanced Cu (II) Removal. *J. Mol. Liq.* **2017**, *230*, 667−673.
(56) Shahrashoub, M.; Bakhtiari, S. The Efficiency of Activated Carbon/Magnetite Nanoparticles Composites in Copper Removal: Industrial Waste Recovery, Green Synthesis, Characterization, and Adsorption-Desorption Studies. *Microporous Mesoporous Mater.* **2021**, *311*, No. 110692.
(57) Sehaqui, H.; de Larraya, U. P.; Liu, P.; Pfenninger, N.; Mathew, A. P.; Zimmermann, T.; Tingaut, P. Enhancing Adsorption of Heavy Metal Ions onto Biobased Nanofibers from Waste Pulp Residues for Application in Wastewater Treatment. *Cellulose* **2014**, *21* (4), 2831−2844.
(58) Kardam, A.; Raj, K. R.; Srivastava, S.; Srivastava, M. M. Nanocellulose Fibers for Biosorption of Cadmium, Nickel, and Lead Ions from Aqueous Solution. *Clean Technol. Environ. Policy* **2014**, *16* (2), 385−393.
(59) Christensen, E. G.; Steele, R. P. Structural, Thermodynamic, and Spectroscopic Evolution in the Hydration of Copper(II) Ions, $Cu^{2+}(H_2O)_{2-8}$. *J. Phys. Chem. A* **2023**, *127* (32), 6660−6676.
(60) Stace, A. J.; Walker, N. R.; Firth, S. $[Cu\cdot(H_2O)_n]^{2+}$ Clusters: The First Evidence of Aqueous Cu(II) in the Gas Phase. *J. Am. Chem. Soc.* **1997**, *119* (42), 10239−10240.
(61) Cui, X.; Lee, J.; Ng, K. R.; Chen, W. N. Food Waste Durian Rind-Derived Cellulose Organohydrogels: Toward Anti-Freezing and Antimicrobial Wound Dressing. *ACS Sustain Chem. Eng.* **2021**, *9* (3), 1304−1312.

https://doi.org/10.1021/acsomega.4c11464
ACS Omega 2025, 10, 6234−6243